Electronic Supplementary Information

for

Critical role of hydrogen bond between microcrystalline cellulose and g-C_3N_4 enables highly efficient photocatalysis

Zhaoqiang Wang[a,†], Guixiang Ding[a,†], Juntao Zhang[a], Xianqing Lv[a], Peng Wang[b], Li Shuai[a], Chunxue Li[c,*], Yonghao Ni[a,*], and Guangfu Liao[a,*]

[a] National Forestry and Grassland Administration Key Laboratory of Plant Fiber Functional Materials, College of Materials Engineering, Fujian Agriculture and Forestry University, Fuzhou 350002, China.

[b]Shandong Chambroad Petrochemicals Co., Ltd, Binzhou, Shandong 256500, China.

[c]College of Ecological Environment and Urban Construction, Fujian University of Technology, Fuzhou 350118, China.

*Corresponding authors. E-mail addresses: chunxueli@fjut.edu.cn (C. Li); yonghao@unb.ca (Y. Ni); liaogf@mail2.sysu.edu.cn (G. Liao)

[†]These authors contributed equally to this work.

Experimental

Experimental materials

All the reagents were of analytical grade and used as received without further purification, Urea (CH_4N_2O, AR 99) was produced from Tianjin Jinhui Taiya Chemical Reagent Co., LTD. Microcrystalline cellulose (MCC), Tetracycline hydrochloride ($C_{22}H_{24}N_2O_8 \cdot HCl$, TC, AR 99) Bisphenol A (BA, AR 99), O-chlorophenol (OCH, AR 98) and 2-Mercaptobenzothiazole (MB, AR 98) was supplied by Aladdin Reagent (Shanghai) Co, Ltd.

Preparation of CN

In a typical synthesis, the urea was ground and dried and calcined in the Muffle furnace at 550 °C for 240 min with heating rate of 2.5 °C min^{-1}. The obtained powder was treated with nitric acid until neutral. After drying at 100 °C for 12 h, sample was calcined in the Muffle furnace at 500 °C for 240 min with heating rate of 5 °C min^{-1}. Remove at room temperature, grind, dry and noted g-C_3N_4 as CN.

Preparation of MCC modified CN

MCC/CN was prepared through dimple physical blending method. In a typical experimental, MCC-X/CN hybrid, where X = 0.01, 0.03, 0.05 and 0.1 g of MCC w.r.t the amount of CN (0.2 g) was dispersed in 100 ml deionized water with vigorous stirring for 24 h. After filtering out the mixture, the samples were dried at 40 °C for 24 h.

Characterization

The scanning electron microscopic (SEM) images were taken on Ultima IV. High-resolution TEM (HRTEM) images were obtained on Jem-2100F. X-ray diffraction (XRD) pattern of samples were carried out via the ULTIMA IV ultima IV diffractometer under Cu Kα radiation at a scanning rate of 5 °C min^{-1} (Japan). UV-vis absorption spectra of samples are measured by U-4150 UV-vis spectrometer (Japan) and Fourier transform infrared spectroscopy (FTIR, Bruker Vertex 70, Germany). The X-Ray photoelectron spectroscopy (XPS) measurements were performed on a VG Microtech Multi lab ESCA3000 spectrometer with a non-monochromatised Mg-Ka X-ray source and energy of 0.8 eV. The binding energy correction was performed by the C1s reference peak of carbon atom at 284.9 eV. The calculation was based on the density functional theory (DFT). All the DFT calculations of model CN, MCC/CN and MCC/CN-Pt were performed with Gaussian 16 (C 01) package suite. The structure of all molecules was optimized by using B3LYP method, the 6-31G (d) basis set was employed for all atoms and water was used to represent the solvents. The frequency calculations were also conducted at the same level of theory to ensure all the optimized structures were at a local minimum on the potential energy surface (PES) and then the generated wave functional files were used to calculate the highest occupied molecular orbital (HOMO) and lowest unoccupied molecular orbital (LUMO) energies. Then, We adopted the TDDFT method, at the B3LYP/6-31G (d) level, to calculate the oscillator strength of the excited states of CN, MCC/CN and MCC/CN-Pt. Adsorption energy analysis were conducted under the MP2 method and the adsorption energy of CN and CN-H were calculated based on the equation: Eads = E_{total} - E_{sub} - E_H, where the E_{sub} and E_H represent the optimal structures of fragmented CTPs and its corresponding energies, respectively. E_{total} is the total energy of the optimal substrates absorbed by H^+.

Photocatalytic degradation test

Firstly, TC, BA, OCH and MB were used as the target molecules to evaluate the photocatalytic degradationactivity of the samples. The photocatalyst (10 mg) was added into target molecules aqueous solution (50 ml) with a concentration of 20 mg/L, and stirred in the dark for 60 min until the adsorption-desorption equilibrium. The photocatalytic degradation was performed by using 300 W Xenon Lamp (Beijing Perfectlight) and UV cut-off filter (λ > 420 nm). s. The concentration of supernatants were determined at the characteristic absorption wavelengths of TC (357 nm), BA (278 nm), OCH (279 nm), MB (322 nm) by U-3900 ultraviolet-visible spectrophotometer with an interval of 15 min. The photo- degradation efficiency and rate constant were obtained as follows:[1]

$$\eta = \frac{C_0 - C}{C_0} \times 100\% \tag{1}$$

$$In\frac{C_0}{C} = K_{app}t \tag{2}$$

where C_0 was the initial concentration, t was the reaction time, C was the concentration at time t, and K_{app} was the first-order rate constant (min^{-1}).

Photocatalytic H_2 evolution activity measurements

The photocatalytic H_2 evolution activity of the obtained samples was evaluated under Labsolar-6A (Beijing Perfectlight). Typically, 25 mg of sample powder is dispersed in an aqueous solution (100 mL) containing triethanolamine (10 vol%) as a sacrifice-electron donor, with the addition of 1.5 ml H_2PtCl_6 (3 wt%). The suspension solution was added into a 150 mL double layered Pyrex reaction cell linked to a circulating cold bath (5 °C). A 300 W Xenon Lamp source (PLS-SXE 300/UV) and UV cut-off filter ($\lambda > 420$) were used for H_2 evolution. The catalyst suspensions were stirred constantly in order to prevent the settling down of the catalyst. Subsequently, an on-line meteorological chromatograph was used to detect the H_2 precipitation rate under visible light irradiation.

Photoelectrochemical test

Photoelectrochemical measurements were conducted in a conventional three-electrode cell system using Chen hua electrochemical station (Shang Hai). The fluorine-doped tin oxide (FTO) transparent conductive film glass deposited with samples, Pt wire, and Ag/AgCl electrode were respectively used as working electrodes, counter electrode, and reference electrode. 0.5 M Na_2SO_4 aqueous solution (pH = 6.8) was used as the electrolyte. In the work, 5.0 mg photocatalyst was well dispersed in 50 μL Nafion PFSA Polymer Dispersions D520 (5%) and 2 ml N, N-dimethylamide ultrasonic for 30 min in an ultrasonic cleaner. Then, evenly drop on the FTO with the glue head dropper, bake in the oven at 40 °C for 5 h, remove the FTO and insert it into the working electrode of the three electrodes. In addition, the photocurrent response of the photocatalysts as light on and off was measured without bias voltage or photocurrent-time curves and electrochemical impedance.

Apparent quantum yield (AQY) measurements

Under the same photocatalytic conditions, using 300W Xenon lamp as light source, monochromatic band-pass filters (420, 450, 500, 550 nm) were used to obtain the required single incident wavelength, and the AQY of H_2 precipitation was measured. The average light intensity was measured by optical power meter (PL-MW2000), and the specific light intensity of 420, 450, 500 and 550 nm was 3.80, 3.84, 2.89 and 4.14 mW cm^{-2}, respectively. After that, catalyst solution was irradiated for 1 h. The AQY was calculated by using the equation:[2]

$$AQY\ (\%) = \frac{(2 \times amount\ of\ H_2\ molecules)}{(Number\ of\ incident\ electrons)} \quad (2 \times M \times A \times h \times c)/(P \times S \times T \times \lambda) \times 100\%$$

(3)

where M is the amount of H_2 molecules (mol), A is the Avogadro constant (6.02×10^{23} mol^{-1}), h is the Planck constant (6.626×10^{-34} m^2 kg s^{-1}), c is the speed of light (3×10^8 m s^{-1}), P is the intensity of irradiation light (W cm^{-2}), S is the irradiation area (cm^2), T is the photoreaction time (s), λ is the wavelength of the monochromatic light (nm).

Figures

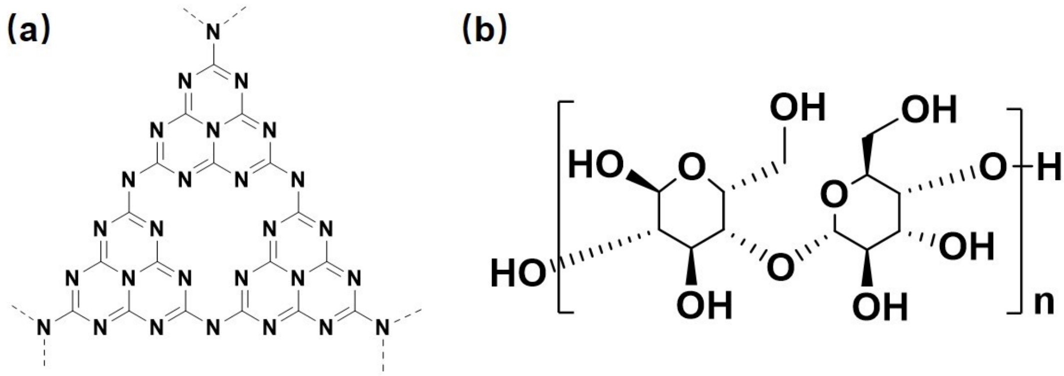

Fig. S1. (a-b) Molecular structure of CN and MCC.

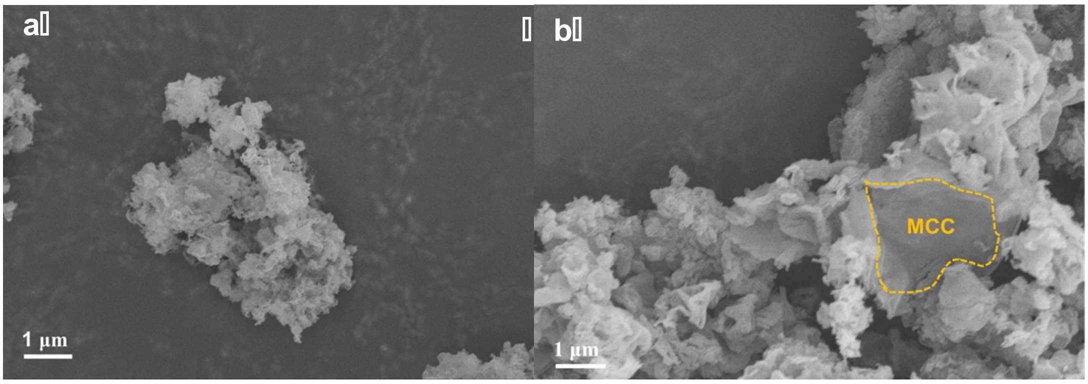

Fig. S2. SEM images of (a) CN and (b) MCC-0.05/CN.

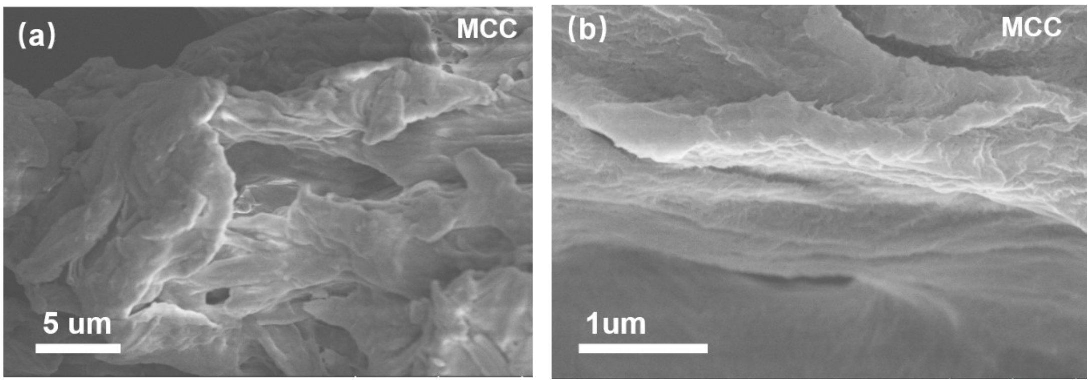

Fig. S3. (a-b) SEM images of MCC.

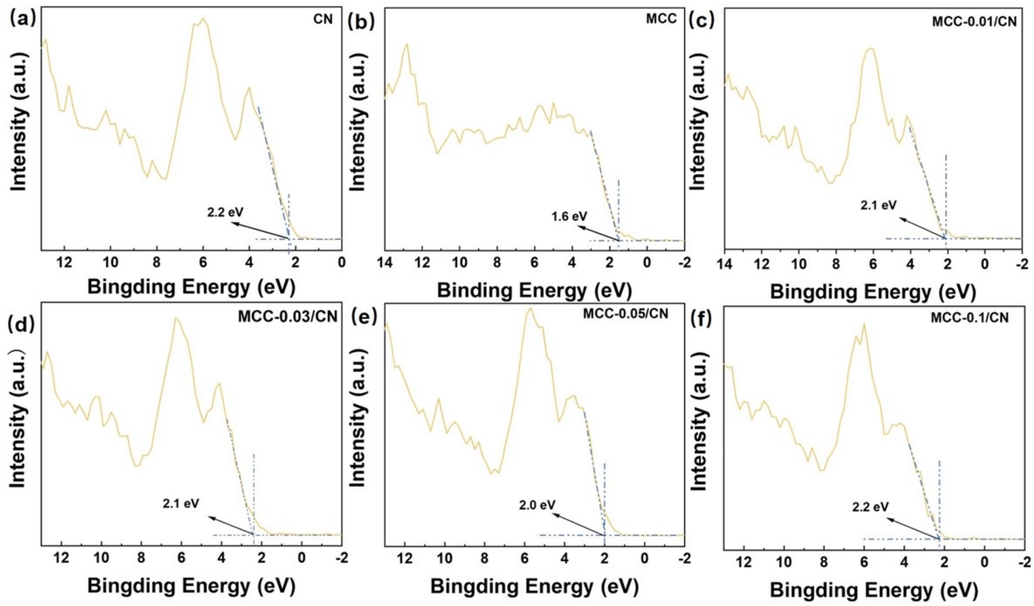

Fig. S4. Valence spectra of different photocatalysts.

As showed in Fig. S3, the bandgap (E_g) was calculated according to Tauc/David-Mott model described by the equation $(\alpha h\nu)^{1/2} = A(h\nu - E_g)$, where h is the Planck constant, v is the frequency of vibration, α is the absorption coefficient, E_g is the bandgap, A is a proportional constant.[3] The bandgap energies of the CN and MCC-X/CN were estimated to be 2.78, 2.77, 2.73, 2.72 and 2.76 eV, respectively. The valence band (E_{VB}) of the CN and MCC-X/CN were determined using valence band X-ray photoelectron spectroscopy (VB-XPS). The E_{VB} position of the CN and MCC-X/CN were estimated to be 2.27, 2.07, 2.07, 1.97 and 2.15 eV via the VB-XPS spectrum. Moreover, the CB positions of the CN and MCC-X/CN were determined to be -0.61, -0.70, -0.76, -0.85 and -0.9 eV according to the empirical formula:

$$E_{CB} = E_{VB} - E_g. \quad (4)$$

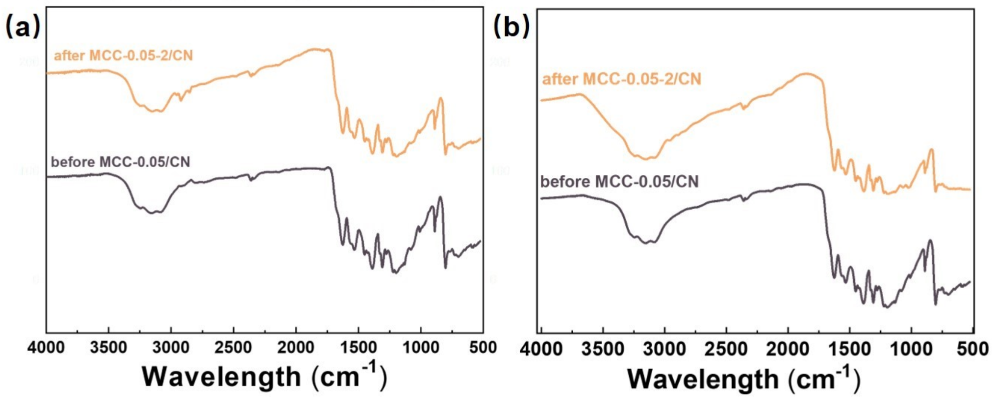

Fig. S5. (a) FTIR spectra of MCC-0.05/CN before and after five cycles during photocatalytic TC degradation experiment. (b) FTIR spectra of MCC-0.05/CN before and after five cycles of during photocatalytic H_2 evolution experiments.

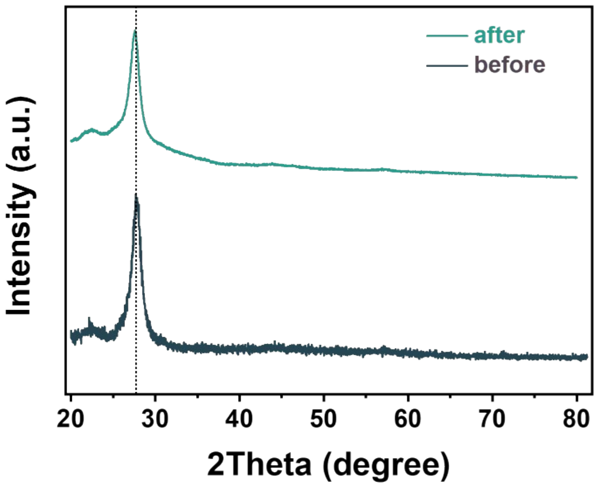

Fig. S6. (a) XRD spectra of MCC-0.05/CN before and after five cycles during photocatalytic TC degradation experiment.

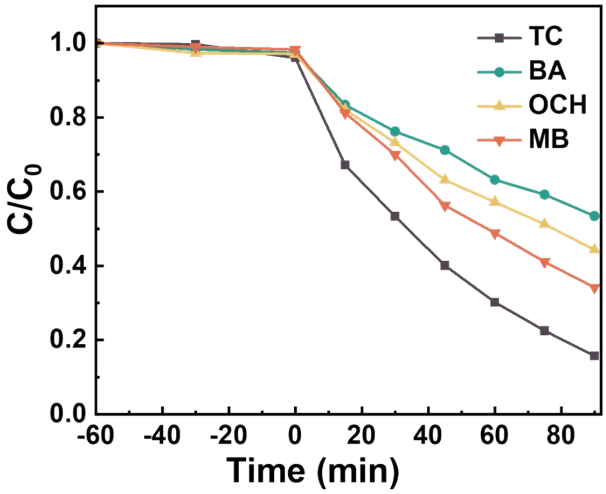

Fig. S7. Degradation dynamic curves of TC, BA, OCH, MB.

For investigating the universal applicability of the MCC-0.05/CN sample for degrading the other various organic pollutants, the photocatalytic degradation experiments of some typical persistent pollutants are further carried out, such as BA, OCH, and MB. As the degradation dynamic curves shown in Fig. S5, the maximal degradation rate of BA, OCH and MB are obtained over the MCC-0.05/CN sample, which reach up to 46.5%, 55.7% and 65.8%, respectively. The results indicate that the MCC-0.05/CN sample has the superior universality for unselective degrading the various organic pollutants

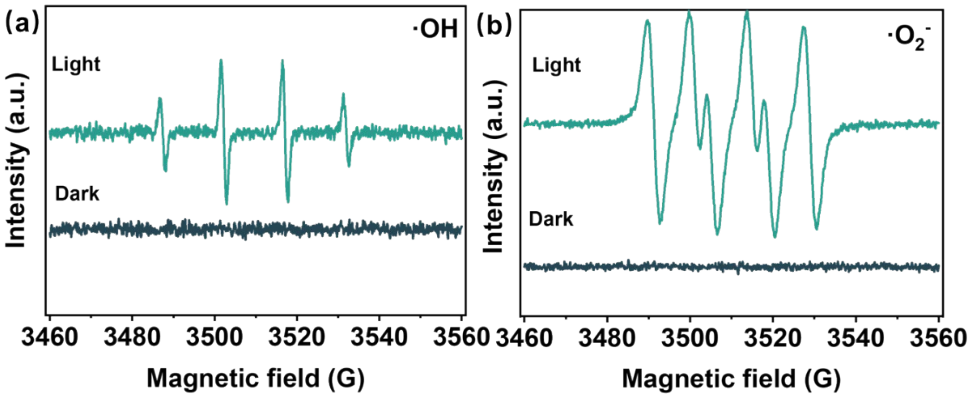

Fig. S8. ESR spectra of ·OH and $\cdot O_2^-$ in the dark and after light irradiation (a, b) for the pristine MCC-0.05/CN.

ESR spectra are detected to capture the signals of generated radicals (·OH and $\cdot O_2^-$) under light irradiation with 5,5-dimethyl-1-pyrroline *N*-oxide (DMPO) as a spin-trapping agent and further revealing the photocatalytic mechanism of MCC-0.05/CN.

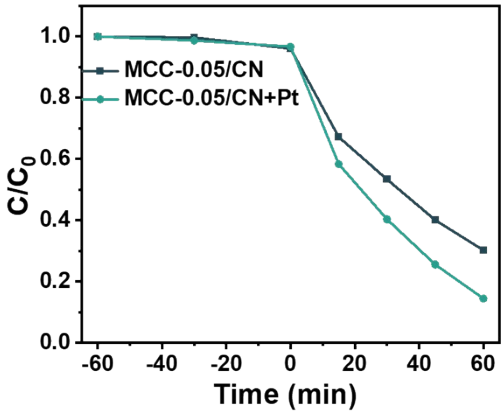

Fig. S9. Photocatalytic degradation curves for TC.

In order to compare the impact of platinum on the degradation of tetracycline, control experiments were conducted using the best samples. The experimental conditions were kept consistent, and 1 mL H_2PtCl_6 (3 wt%) was added to one set of experiments. Figure S8 illustrated that the degradation rate of the catalyst increased from 69.8% to 86.6% when platinum was introduced. The results showed that platinum accelerates the degradation of tetracycline

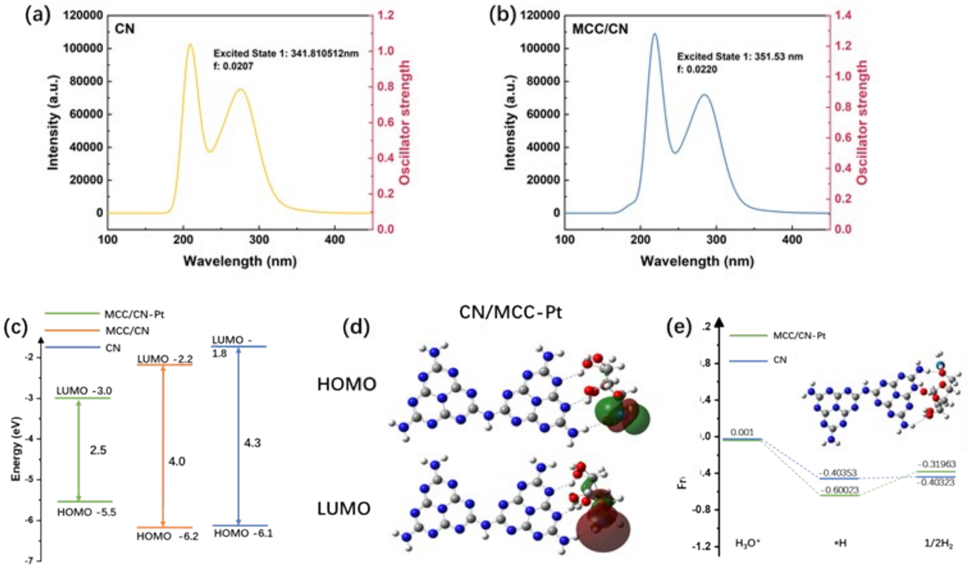

Fig. S10. (a, b) TD-DFT-calculated absorption spectra and oscillator strengths for the model system of CN and MCC/CN at the initial state; (c) Calculated HOMO/LUMO energy levels of MCC/CN-Pt; (d) HOMO/LUMO distributions of MCC/CN-Pt; (e) Calculated free energy diagrams of H_2 production catalyzed by CN and MCC/CN model system.

Tables

Table S1. The activity comparison of the photocatalytic TC degradation of CN-based photocatalysts.

Photocatalyst	Efficiency % (time)	$^{a}K_{app}$ (min^{-1})	Catalyst; TC	Conditions	Ref.
$ZnO/g-C_3N_4$	78.4 (50 min)	0.1490	20 mg; 20 mg /L	Xl 300 W (λ ≥ 400 nm)	[4]
B-PCN	81.3 (120 min)	0.0170	10 mg; 40 mg/L	Xl 300 W (λ ≥ 420 nm	[5]
$Nv-g-C_3N_4$	78.0 (120 min)	0.0100	50 mg; 20 mg/L	LED 50 W	[6]
$WO_3@g-C_3N_4$ @MWCNs	79.5 (120 min)	0.0172	20 mg; 20 mg/L	Halogen lamp 500 W (λ ≥ 420 nm	[7]
$Ag/g-C_3N_4$	83.0 (120 min)	-	100 mg; 20 mg/L	Xl 300 W (λ ≥ 420 nm)	[8]
$WO_3/g-C_3N_4$	70.0 (120 min)	0.0120	50 mg; 25 mg/L	Xl 300 (λ ≥ 420 nm)	[9]
BrCN	75.0 (150 min)	0.0179	250 mg; 10mg/L	LED lamp 38.5 W (λ > 450 nm)	[10]
CQDs/ $g-C_3N_4$	78.6 (240 min)	0.0064	50 mg; 10 mg/L	Xl 250 W (λ ≥ 420 nm)	[11]
$ZnSnO_3$/CN	85.0 (120 min)	0.0131	25 mg; 10 mg/L	Xl 300 W (λ ≥ 400 nm)	[12]
CFs/$g-C_3N_4$/ BiOB	86.1 (120 min)	0.0150	15 mg; 20 mg/L	Xl 300 W (λ ≥ 400 nm)	[13]
h-BN/WO_3/g-C_3N_4	88.5 (120 min)	0.0130	50 mg; 10 mg/L	Xl 300 W (λ ≥ 420 nm)	[14]
$V_2O_5/g-C_3N_4$	75.0 (120 min)	-	50 mg; 10 mg/L	Xl 300 W (λ ≥ 420 nm)	[15]
NCNT/mpg-C_3N_4	67.1	-	20 mg; 10mg/L	Xl 300 W (λ ≥ 400 nm)	[16]
$Bi_2WO_6/g-C_3N_4$	73.0 (60 min)	0.0345	50 mg; 10 mg/L	Xl 250 W (λ ≥ 420 nm)	[17]
HDMP-$g-C_3N_4$	74.0 (60 min)	0.0101	10 mg; 20 mg/L	Xl 300 W (λ ≥ 420 nm)	[18]
$Nb_2O_5/g-C_3N_4$	76.2 (150 min)	0.0096	50 mg; 10 mg/L	Xl 250 W (λ ≥ 420 nm)	[19]
MCC-0.05/CN	84.24 (90 min)	0.019	10 mg; 20 mg/L	Xl 300W (λ ≥ 420 nm)	This work

$^{a}K_{app}$: the first-order rate constant (min^{-1}).

Table S2. The activity comparison of the photocatalytic H_2 production of CN-based photocatalysts.

Photocatalyst	H_2 evolution rate (μmol h^{-1} g^{-1})	Reaction conditions	Light source	Ref.
BP/g-C_3N_4	101	MeOH	Xl (λ ≥ 420 nm)	[20]
CNQDs/CoPi	234.5	TEOA	Halogen lamp (λ ≥ 420 nm)	[21]
BP/g-C_3N_4	384.2	TEOA	Xl (λ ≥ 420 nm)	[22]
NiCoP/g-C_3N_4	159	MeOH	UV-vis light irradiation	[23]
m-gCN/BP-M	442	TEOA	Solar Light (λ ≥ 420 nm)	[24]
Zn-MOFs/g-C_3N_4	484.1	TEOA	Xl 300W (λ ≥ 420 nm)	[25]
MIL-125/g-C_3N_4	606	TEOA	Xl 298W (λ ≥ 420 nm)	[26]
Co/Mo-MCN.	694.5	TEOA	Xl (λ ≥ 420 nm)	[27]
BPQDs/g-C_3N_4	271.0	MeOH	Visible-Light	[28]
BP/g-C_3N_4	571	Lactic acid	Xl 300W (λ ≥ 400 nm)	[29]
2D BP/2D C_3N_4	259.04	-	Xl 300W (λ ≥ 400 nm)	[30]
NYFG/C_3N_4 NT	311.6	TEOA	Xl 300W	[31]
g-C_3N_4–ZnCdS	108.9	Na_2S; Na_2SO_3	Xl 300W (λ ≥ 420 nm)	[32]
Ag/CoxP/Meso-g-C_3N_4	96.66	-	Xl 300W (λ ≥ 420 nm)	[33]
MCC-0.05/CN	642.71	TEOA	Xe lamp 300W (λ ≥ 420 nm)	This work

Reference

1. C. Wang, R. Yan, M. Cai, Y. Liu and S. Li, *Appl. Surf. Sci.*, 2023, **610**, 155346.
2. H. Che, C. Liu, G. Che, G. Liao, H. Dong, C. Li, N. Song and C. Li, *Nano Energy*, 2020, **67**, 104273.
3. M. Shafaee, E. K. Goharshadi, M. Mashreghi and M. Sadeghinia, *J. Photochem. Photobiol. A: Chem.*, 2018, **357**, 90-102.
4. H. Jingyu, Y. Ran, L. Zhaohui, S. Yuanqiang, Q. Lingbo and A. Nti Kani, *Solid State Sci.*, 2019, **92**, 60-67.
5. T. Zhou, T. Li, J. Hou, Y. Wang, B. Hu, D. Sun, Y. Wu, W. Jiang, G. Che and C. Liu, *Chem. Eng. J.*, 2022, **445**, 136643.
6. U. Ghosh, A. Majumdar and A. Pal, *Mater. Res. Bull.*, 2021, **133**, 111074.
7. V. S. Manikandan, S. Harish, J. Archana and M. Navaneethan, *Chemosphere*, 2022, **287**, 132050.
8. Z. Ren, F. Chen, K. Wen and J. Lu, *J. Photochem. Photobiol. A: Chem.*, 2020, **389**, 112217.
9. T. Xiao, Z. Tang, Y. Yang, L. Tang, Y. Zhou and Z. Zou, *Appl. Catal. B: Environ.*, 2018, **220**, 417-428.
10. J. Hong, D. K. Hwang, R. Selvaraj and Y. Kim, *J. Ind. Eng. Chem.*, 2019, **79**, 473-481.
11. Y. Hong, Y. Meng, G. Zhang, B. Yin, Y. Zhao, W. Shi and C. Li, *Sep. Purif. Technol.*, 2016, **171**, 229-237.
12. X. Huang, F. Guo, M. Li, H. Ren, Y. Shi and L. Chen, *Sep. Purif. Technol.*, 2020, **230**, 115854.
13. Z. Shi, Y. Zhang, X. Shen, G. Duoerkun, B. Zhu, L. Zhang, M. Li and Z. Chen, *Chem. Eng. J.*, 2020, **386**, 124010.
14. Y. Yang, B. Liu, J. Xu, Q. Wang, X. Wang, G. Lv and J. Zhou, *ACS Omega*, 2022, **7**, 6035-6045.
15. Y. Hong, Y. Jiang, C. Li, W. Fan, X. Yan, M. Yan and W. Shi, *Appl. Catal. B: Environ.*, 2016, **180**, 663-673.
16. J. Liu, Y. Song, H. Xu, X. Zhu, J. Lian, Y. Xu, Y. Zhao, L. Huang, H. Ji and H. Li, *J. Colloid Interface Sci.*, 2017, **494**, 38-46.
17. H. Che, C. Liu, W. Hu, H. Hu, J. Li, J. Dou, W. Shi, C. Li and H. Dong, *Catal. Sci. Technol.*, 2018, **8**, 622-631.
18. Y. Lin, L. Wang, Y. Yu, X. Zhang, Y. Yang, W. Guo, R. Zhang, Y. Zhai and Y. Liu, *New J. Chem.*, 2021, **45**, 18598-18608.
19. Y. Hong, C. Li, G. Zhang, Y. Meng, B. Yin, Y. Zhao and W. Shi, *Chem. Eng. J.*, 2016, **299**, 74-84.
20. M. Zhu, S. Kim, L. Mao, M. Fujitsuka, J. Zhang, X. Wang and T. Majima, *J. Am. Chem. Soc.*, 2017, **139**, 13234-13242.
21. X. Liu, L. Hu, Y. Zhang, H. Lai, G. Peng, J. Li, R. Zeng and Z. Yi, *Photochem. Photobiol.*, 2023, 1751-1097.
22. Q. Zhang, S. Huang, J. Deng, D. T. Gangadharan, F. Yang, Z. Xu, G. Giorgi,

M. Palummo, M. Chaker and D. Ma, *Adv. Funct. Mater.*, 2019, **29**, 1616-3028.
23. B. Ma, J. Zhao, Z. Ge, Y. Chen and Z. Yuan, *Sci. China Mater.*, 2019, **63**, 258-266.
24. S. Yılmaz, E. G. Acar, G. Yanalak, E. Aslan, M. Kılıç, İ. Hatay Patır and Ö. Metin, *Appl. Surf. Sci.*, 2022, **593**, 153398.
25. H. Gao, J. Xu, J. Zhou, S. Zhang and R. Zhou, *J. Colloid Interface Sci.*, 2020, **570**, 125-134.
26. C. Wei, W. Zhang, X. Wang, A. Li, J. Guo and B. Liu, *Catal. Lett.*, 2020, **151**, 1961-1975.
27. W. Wu, Z. Ruan, J. Li, Y. Li, Y. Jiang, X. Xu, D. Li, Y. Yuan and K. Lin, *Nano-Micro Lett.*, 2019, **11**, 2150-5551.
28. W. Lei, Y. Mi, R. Feng, P. Liu, S. Hu, J. Yu, X. Liu, J. A. Rodriguez, J.-o. Wang, L. Zheng, K. Tang, S. Zhu, G. Liu and M. Liu, *Nano Energy*, 2018, **50**, 552-561.
29. J. Ran, W. Guo, H. Wang, B. Zhu, J. Yu and S. Z. Qiao, *Adv. Mater.*, 2018, **30**, 0935-9648.
30. X. Zhang, J. Deng, J. Yan, Y. Song, Z. Mo, J. Qian, X. Wu, S. Yuan, H. Li and H. Xu, *Appl. Surf. Sci.*, 2019, **490**, 117-123.
31. Y. Zhu, X. Zheng, Y. Lu, X. Yang, A. Kheradmand and Y. Jiang, *Nanoscale*, 2019, **11**, 20274-20283.
32. A. B. Yousaf, M. Imran, M. Farooq, S. Kausar, S. Yasmeen and P. Kasak, *Nanomaterials*, 2023, **13**, 2609.
33. Z. Yang, Z. Xing, D. Chi, Z. Li, D. Sun, X. Du, J. Yin and W. Zhou, *Nanotechnology*, 2019, **30**, 485401.